

Oscillatory neck propagation in polymer films: a novel model and its refinements

Wenjie Fan
Keble College
University of Oxford

A report of summer project supervised by
Prof. Ed Brambley
University of Warwick

Summer 2022

Contents

1	Introduction	1
1.1	Stress Oscillation	1
1.2	Barenblatt's model [4]	2
1.3	Toda's model [5]	4
1.4	Generalised Toda's model [1]	5
1.4.1	Stress equation	6
1.4.2	Neck propagation speed	7
1.4.3	Heat balance equation	7
1.4.4	Eyring's equation	9
1.5	Numerical scheme – finite volume method	9
2	Tuning parameters	12
2.1	Effects of changing individual parameters	13
2.1.1	Varying E_0	13
2.1.2	Varying E_1	14
2.1.3	Varying ΔF	14
2.1.4	Varying α	15
2.1.5	Varying ρ	15
2.1.6	Varying k_i	16
2.1.7	Varying v_0	17
2.1.8	Varying c_p	18
2.1.9	Varying h_i	19
2.1.10	Varying λ	21
2.1.11	Varying η	22
2.2	Further suggestions on fitting parameters	23
2.2.1	Combining ΔF and α	23
2.2.2	Sensitivities of parameters and fitting	23
2.3	Simulation results and discussion	24

3	Introducing density change	27
3.1	Re-derivation of governing equations	27
3.2	Numerical scheme of the new model	28
3.3	Effect of the second density	30
3.4	Comparison with the experiments	31
4	Conclusion	33
A	Derivation: steady states of the new model	35
B	Comparison of predicted critical compliance	37
	Bibliography	39

List of Figures

1.1	A photo taken by camera during the experiments.	2
1.2	A sketch explaining Eyring's equation in a transition state model's view.	3
1.3	A slice from the sample.	4
1.4	A schematic for the propagation process, captured when there's no elasticity. The actual case is the undeformed region has two parts, one at the left and one at the right, due to symmetry. We did the simplification here, illustrating it one-side. [1]	5
1.5	Illustrate of the sample over a short time period Δt , assuming there's currently no load applied on it. ν denotes the speed of neck propagation (plastic deformation).	7
1.6	A schematic for the modelling of heat transfer in the sample, taking a slice. $J(x, t)$ is the thermal diffusion flux density, Ω is the volume between x_1 and x_2 . [1]	8
1.7	A schematic for the elements we considered in finite volume method. In simulation we will also have time step $\Delta t = 0.005\text{s}$, where for each time we have temperature of each block in the schematic recorded (so that there will be a matrix). Two temperatures at $j = -3, 3$ are for illustration purpose. Other variables will be stored in array from, determined by time t solely.	9
2.1	Comparison of numerical and experimental results, using the parameters proposed by Nathan.	13
2.2	Varying E_0 , retaining the top-left.	13
2.3	Varying E_1 , with the inset a closer look.	14
2.4	Varying ΔF , with the inset a closer look.	14
2.5	Varying α , giving similar effect as ΔF	15
2.6	Varying ρ , with the inset a closer look.	15
2.7	Varying k_0 and k_1 simultaneously.	16

2.8	Temperature intensity plot with Left: $k_0 = k_1 = 1.5 \times 10^4 \text{ erg cm}^{-1} \text{ s}^{-1} \text{ K}^{-1}$, and Right: $k_0 = k_1 = 2 \times 10^4 \text{ erg cm}^{-1} \text{ s}^{-1} \text{ K}^{-1}$	16
2.9	Different k_0 and k_1 , retaining k_0 while controlling the ratio.	17
2.10	Varying v_0 causes lift in the stress curve.	17
2.11	Varying c_p	18
2.12	Temperature intensity plot with Left: $c_p = 1.12 \times 10^7 \text{ erg g}^{-1} \text{ K}^{-1}$, and Right: $c_p = 0.8 \times 10^7 \text{ erg g}^{-1} \text{ K}^{-1}$	18
2.13	Approximated temperature at neck front against time. Comparing two different heat capacities.	19
2.14	Varying h_0 and h_1 simultaneously.	19
2.15	Fixing h_0 , while varying the ratio of h_0 and h_1	20
2.16	Temperature intensity plot with Left: $h_0 = h_1 = 2.33 \times 10^3 (\text{erg cm}^{-2} \text{ s}^{-1} \text{ K}^{-1})$, and Right: $h_0 = h_1 = 8.33 \times 10^3 (\text{erg cm}^{-2} \text{ s}^{-1} \text{ K}^{-1})$	20
2.17	Temperature at neck front against time. Comparing two different sets of heat loss rate from sample to air.	21
2.18	Varying λ , The case $\lambda = 2$ was the value Toda used where conse- quently the speed of neck propagation $ \dot{\chi} $ equals the speed of plastic deformation ν	21
2.19	Varying η	22
2.20	Temperature intensity plot with Left: $\eta = 1.0$, and Right: $\eta = 0.6$	22
2.21	Temperature at neck front against time. Comparing two different con- version efficiency from mechanical work to heat.	23
2.22	Comparison of two sets of values for ΔF and α . The yield point is preserved while the average stress can be adjusted.	23
2.23	Simulation results with the proposed parameters in Chapter 1.	25
3.1	A comparison of the effect of bringing in the second density, assuming $\rho_1 = 0.8 \text{ cm s}^{-1}$	30
3.2	With two densities, setting unusually high value for ρ_0 can suppress the oscillation at the beginning.	31
3.3	Simulation with parameter from Chapter 2, adding the second density $\rho_1 = 0.9 \text{ g cm}^{-1}$	31
3.4	Stress-Strain curves of different materials, omitting strain $> 200\%$. Again this is because we are only interested in the parts before the rise in stress and that's strain $< 200\%$	32

Chapter 1

Introduction

The summer project is continuing previous students' work. Among them the latest one is Nathan's thesis for master's degree, *Oscillatory neck propagation in polymer films* [1]. To facilitates the report, we will cover some introductions to the problem in this chapter, as well as major models related.

1.1 Stress Oscillation

The problem was posed by Chaoying Wan, et al. from the Warwick Manufacturing Group, with a set of experimental data and an example video. Imaging stretching a rectangular film made of polyethylene terephthalate (PET), sometimes the plastic deformation is violent and then it break instantly. While for this project we examine the weird case where the polymer film doesn't break immediately. In this case, band pattern consists of opaque and translucent stripes arises, and stress oscillates.

One of the experiments is shown in Figure 1.1. The banding pattern in the bottom is an obvious manifestation of stress oscillation. One can see the region with banding pattern is slightly narrower, where the sample has been plastically deformed. The region has a smaller width and thickness and is called the **neck**. The remaining part is called the **undeformed region**. The tiny region connecting the above two regions are considered infinitesimal in our modelling, and we called it the **neck front**. One may also observe from the figure that the sample is of a dog-bone shape, with both ends wider. This is for the clamps to hold the sample tightly and to ensure the stretch is even. In experimental results presented later, we may see the stress-strain curve has a increase for large strains. This is thus an experimental feature and will not be accounted in our prediction.



Figure 1.1: A photo taken by camera during the experiments.

There were several models explaining this phenomenon. Toda's model, although simple (and has some ambiguity), was proved to be the most accurate by far. The first paper in 1993 presented a review and analysis on Barenblatt's model which was proposed in 1970s. The model has a quite complete modelling on stress but for temperature it only considers changes at the neck front [4]. Later in 1994, Toda introduced spatial temperature distribution along the sample and achieved great results in his second paper [5].

1.2 Barenblatt's model [4]

Barenblatt's model assumes all the work done is converted to heat at the neck front. So that everywhere (including air) has a temperature T_a , except $T_0(t)$ at the neck front. The heat balance equation is thus:

$$\rho c_p \Omega \frac{dT_0}{dt} = -\underbrace{\rho c_p S_0 v (T_0 - T_a)}_1 - \underbrace{h A (T_0 - T_a)}_2 + \underbrace{S_0 \sigma v}_3 \quad (1.1)$$

where we have variables: neck front temperature $T_0(t)$, neck front normal stress $\sigma(t)$, and neck front velocity $v(t)$. Besides we have: mass density ρ , heat capacity c_p , neck front volume Ω , undeformed cross sectional area S_0 , heat transfer coefficient (along the sample) h , and neck front surface area A . The equation considers the conservation of rate of change in heat, where the left hand side is the rate at neck front, and the three terms in the right can be interpreted as follows:

1. Rate of heat transfer from neck front to new propagated parts of the neck
2. Rate of heat conduction to other parts and loss to air
3. Rate of mechanical work converting to heat at neck front

With three variables, we need two another equations to solve the system. The first equation is a stress-strain relation

$$\frac{d\sigma}{dt} = \frac{V - v}{D} \quad (1.2)$$

where V is the speed of drawing¹, and D is a material constant (later the *system elastic compliance*). We will have a rigorous derivation of equation 1.2 later. The third equation is an application of Eyring process, Eyring's equation:

$$v = v_0 \exp \left[\frac{-(\Delta F - \alpha\sigma)}{k_B T_0} \right] - v_0 \exp \left[\frac{-(\Delta F + \alpha\sigma)}{k_B T_0} \right] \quad (1.3)$$

It has been experimentally confirmed by Toda that the above logarithm relation between v and $1/T_0$ makes sense [3]. An intuitive way to understand the equation is to refer to the transition state model, where one assumes a transition happens when the thermodynamic free energy exceeds an activation barrier ΔF . This barrier ΔF is subject to change when stress exists, and we assume the shift is $\alpha\sigma$, proportional to the stress. The shifted barrier for the undeformed region is $\Delta F - \alpha\sigma$, smaller than $\Delta F + \alpha\sigma$ for the neck. So that statistically mechanically, there's a trend for polymer chain movement towards the neck. Figure 1.2 illustrates this, where the black curve is the case when no load is applied.

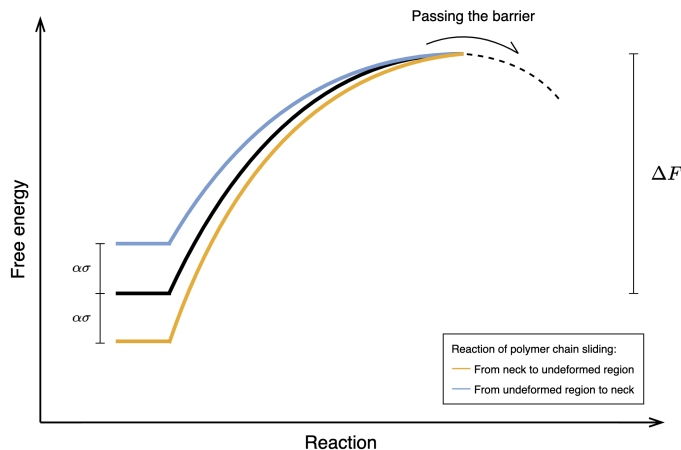


Figure 1.2: A sketch explaining Eyring's equation in a transition state model's view.

¹Throughout the report, we assume that the sample is draw at a constant rate.

Barenblatt's model cast heat on the neck front only, which is not realistic: there is a jump in temperature within the sample. A more favourable method is to introduce temperature distribution along the sample, where the temperature $T(x, t)$ will become a function of both displacement and time. This idea takes us to Toda's model.

1.3 Toda's model [5]

Toda modelled the strip sample by a cuboid, of width a and thickness b . Below is a slice taken from the sample where we consider the thermal energy per volume on.

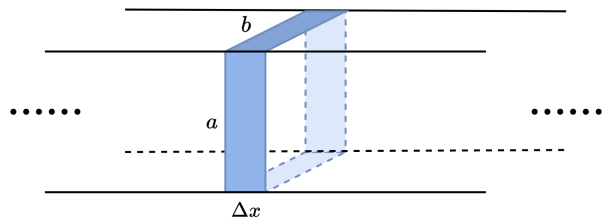


Figure 1.3: A slice from the sample.

Taking the frame moving with neck front, i.e. $x = 0$ consistently at the neck front, and balancing the rate of change of thermal energy per unit volume:

$$\begin{aligned} \left(\frac{\partial}{\partial t} + v \frac{\partial}{\partial x} \right) (c_p \rho T) &= k \frac{\partial^2 T}{\partial x^2} - (T - T_a) h \frac{(2a + 2b)\Delta x}{ab\Delta x} + \frac{\sigma abv}{ab\Delta x} \\ \implies \rho c_p \left(\frac{\partial}{\partial t} + v \frac{\partial}{\partial x} \right) T &= -h \left(\frac{1}{a} + \frac{1}{b} \right) (T - T_a) + k \frac{\partial^2 T}{\partial x^2} + \eta \sigma v \delta(x) \end{aligned} \quad (1.4)$$

where η is the efficiency of work converting to heat. We have abbreviated a coefficient 2 on the second term in the right into h , and write $1/\Delta x$ as $\delta(x)$ by taking $\Delta x \rightarrow 0$. The first bracket on the left hand side is the advection operator accounting frame movement. The most noteworthy point here is, Toda seems ambiguously used the velocity of neck front and the speed of drawing, setting both of them to be v . The two speeds are different and we will have a rigorous discussion in Section 1.4.2.

The other two equations needed to solve this system remain unchanged:

$$\frac{d\sigma}{dt} = \frac{V - v}{D} \quad (1.5)$$

$$v = v_0 \exp \left[\frac{-(\Delta F - \alpha\sigma)}{k_B T_0} \right] - v_0 \exp \left[\frac{-(\Delta F + \alpha\sigma)}{k_B T_0} \right] \quad (1.6)$$

where $T_0(t) := T(0, t)$ is the temperature at neck front.

According to analytic derivation (see Section 1.4), some assumptions are needed to make the system of equation valid and coincides with the experiments:

- Due to the ambiguous usage of v , the problem is asserting some restrictions. We will see in the next section that this implies that the ratio of mass between the undeformed and deformed parts is 2.
- Compliance D is assumed to be a constant. Later we will see that D should be a variable related to the initial length, the stage of neck propagation, and the elastic moduli.
- $\frac{\sigma}{E_0} \left(1 - \lambda^2 \frac{E_0}{E_1}\right) \rightarrow 0$, presumably $\sigma \ll E_0$ the elastic modulus of the undeformed region. Indeed $E_0 \approx 2.5\text{GPa}$ and $\sigma \approx 20\text{MPa}$, so this is not a problem.

Despite the above assumptions, a fatal flaw is that the model is not conserving mass generally: since Toda assigned constant value a and b to both the deformed part and the undeformed part. This will be fixed in the Generalised model by Nathan.

1.4 Generalised Toda's model [1]

We start with the setup of the model. Define $\chi(t)$ and $L(t)$ to be the length of the undeformed region and the length of the total sample, both without elastic deformation (not stretched). While during the experiment, we denote $l_0(t)$ and $l_1(t)$ to be the length of the undeformed parts and deformed parts respectively. Assume S_i and σ_i the cross sectional area and stress for two regions, where $i = 0, 1$ as annotated in the diagram below.

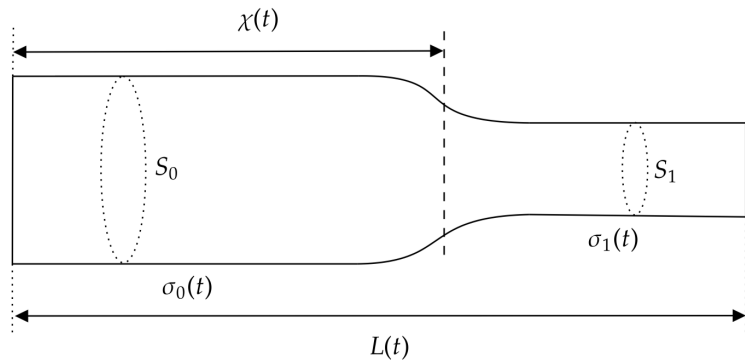


Figure 1.4: A schematic for the propagation process, captured when there's no elasticity. The actual case is the undeformed region has two parts, one at the left and one at the right, due to symmetry. We did the simplification here, illustrating it one-side. [1]

1.4.1 Stress equation

Regardless of the neck front where plastic deformation takes place, we can model the material as elastic solids. Hence by the definition of Young's modulus E_0, E_1 we have the following for the undeformed parts and neck respectively:

$$E_0 = \frac{\sigma_0}{\epsilon_0} = \frac{\chi\sigma_0}{l_0 - \chi}, \quad E_1 = \frac{\sigma_1}{\epsilon_1} = \frac{(L - \chi)\sigma_1}{l_1 - (L - \chi)},$$

By conservation of mass,

$$\rho_0 S_0 L_0 = \rho_0 S_0 \chi + \rho_1 S_1 (L - \chi)$$

Define $\lambda := \rho_0 S_0 / \rho_1 S_1$ to be the **draw ratio**, then $L = \chi + \lambda(L_0 - \chi)$, so that:

$$l_0 = \chi \left(\frac{\sigma_0}{E_0} + 1 \right), \quad l_1 = \lambda(L_0 - \chi) \left(\frac{\sigma_1}{E_1} + 1 \right) \quad (*)$$

Now we make probably the most restrictive assumption of Nathan's model: $\rho_0 = \rho_1$. This is a risky decision and we will see what happens if we relax this constraints in Chapter 3. Now $\lambda = S_0/S_1$ hence by $F = S_0\sigma_0 = S_1\sigma_1$ we get:

$$\lambda\sigma_0 = \sigma_1 \quad (**)$$

We can now represent σ_1 in terms of σ_0 solely. We will do so, and will discuss σ_0 only from now on. By $(*)$ we can get an expression for the draw rate:

$$V = \dot{l}_0 + \dot{l}_1 = \dot{\chi} \left\{ \frac{\sigma_0}{E_0} - \lambda \frac{\sigma_1}{E_1} + (1 - \lambda) \right\} + \chi \frac{\dot{\sigma}_0}{E_0} + \lambda(L_0 - \chi) \frac{\dot{\sigma}_1}{E_1}$$

By $(**)$ with some further calculations (notice that $\dot{\chi} < 0$, since polymer chains are sliding away), we get the new equation to 1.5,

$$\dot{\sigma}_0 = \frac{1}{D(\chi; L_0)} \left\{ V - |\dot{\chi}| \left[\frac{\sigma_0}{E_0} \left(\lambda^2 \frac{E_0}{E_1} - 1 \right) + (\lambda - 1) \right] \right\} \quad (1.7)$$

where we have rigorously introduced the **System elastic compliance**, in replacing of the previous constant D :

$$D(\chi; L_0) := \frac{\chi}{E_0} + \lambda^2 \frac{L_0 - \chi}{E_1}$$

This definition seems to be incomplete facing density change, see Chapter 3.

1.4.2 Neck propagation speed

In this subsection we will rigorously derive the speed of plastic deformation and the velocity needed in the advection term in the diffusion operator. This will then give a correction to Toda's model.

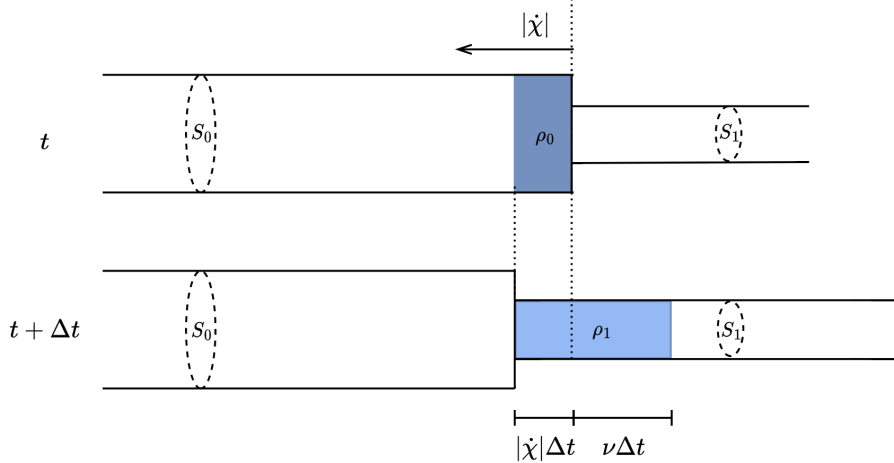


Figure 1.5: Illustrate of the sample over a short time period Δt , assuming there's currently no load applied on it. ν denotes the speed of neck propagation (plastic deformation).

As illustrated above, the dark blue region is changed to the light blue region over the time step Δt , with some plastic deformation. While the other parts remain unchanged if there's no load, as we model them by elastic solids. By the conservation of mass, with $\rho_0 = \rho_1$,

$$S_0 \rho_0 |\dot{\chi}| \Delta t = S_1 \rho_1 (|\dot{\chi}| + \nu) \Delta t \implies \nu = (\lambda - 1) |\dot{\chi}|$$

Referring to Figure 1.5, the undeformed parts moves in a positive direction with speed $|\dot{\chi}|$ relative to the neck front $x = 0$, while the neck moves similarly with speed $|\dot{\chi}| + \nu$. Thus the advection speed for these parts are just the speeds respectively. Combining these gives the diffusion operator:

$$\frac{\partial}{\partial t} + (1 + H(x)(\lambda - 1)) |\dot{\chi}| \frac{\partial}{\partial x}$$

1.4.3 Heat balance equation

When we model the difference in width and thickness, everything is related to displacement x , thus some parameters need to be changed to functions. We define $\tau(x, t) := T(x, t) - T_a$ as the temperature difference with the air. Note that in some circumstances we have equivalences, e.g. $\frac{\partial T}{\partial t} = \frac{\partial \tau}{\partial t}$. Consider the following schematic:

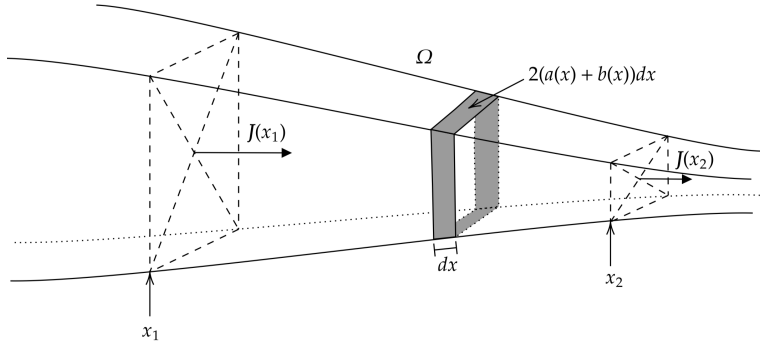


Figure 1.6: A schematic for the modelling of heat transfer in the sample, taking a slice. $J(x, t)$ is the thermal diffusion flux density, Ω is the volume between x_1 and x_2 . [1]

In our approximation, the cross-sectional area $S(x)$ is just $a(x)b(x)$. By Fick's law of diffusion, $J(x, t) = -k(x)\frac{\partial T}{\partial x}(x, t)$. Consider the rate of heat change for the control volume Ω , and assume temporarily that there's no advection,

$$\begin{aligned} & \frac{d}{dt} \int_{\Omega} \rho c_p T(x, t) dV \\ &= \int_{x_1}^{x_2} S(x) \rho c_p \frac{\partial T}{\partial t}(x, t) dx \\ &= - \int_{x_1}^{x_2} h(x)(a(x) + b(x))(T(x, t) - T_a) dx - [S(x_2) J(x_2, t) + S(x_1) J(x_1, t)] \\ &= \int_{x_1}^{x_2} \left\{ -h(x)(a(x) + b(x))(T(x, t) - T_a) + \frac{\partial}{\partial x} \left(S(x) k(x) \frac{\partial T}{\partial x}(x, t) \right) \right\} dx \end{aligned}$$

Read the second and the last line,

$$S \rho c_p \frac{\partial T}{\partial t} = -r(T - T_a) + \frac{\partial}{\partial x} \left(\kappa \frac{\partial T}{\partial x} \right)$$

where $r(x) := h(x)(a(x)+b(x))$ and $\kappa(x) := S(x)k(x)$. The functions can be simplified using heaviside functions:

$$\begin{aligned} S(x) &= S_0 H(-x) + S_1 H(x) \\ r(x) &= h_0 (a_0 + b_0) H(-x) + h_1 (a_1 + b_1) H(x) \\ \kappa(x) &= S_0 k_0 H(-x) + S_1 k_1 H(x) \end{aligned}$$

Recall that the neck front has heat supply rate $\eta S_0 \sigma_0 (\lambda - 1) |\dot{\chi}| \delta(x)$, where $\delta(x)$ is the Dirac delta function. With this section and section 1.4.2, the complete version of heat balance equation is:

$$\begin{aligned} & S \rho c_p \left(\frac{\partial T}{\partial t} + (1 + H(x)(\lambda - 1)) |\dot{\chi}| \frac{\partial T}{\partial x} \right) \\ &= -r(T - T_a) + \frac{\partial}{\partial x} \left(\kappa \frac{\partial T}{\partial x} \right) + S_0 \eta (\lambda - 1) |\dot{\chi}| \sigma_0 \delta(x) \end{aligned} \quad (1.8)$$

1.4.4 Eyring's equation

We applied Eyring's equation to model the plastic deformation rate, which is ν in our new context. We now have the relation $\nu = (\lambda - 1)|\dot{\chi}|$, so that:

$$|\dot{\chi}| = \frac{2v_0}{\lambda - 1} \exp \left[\frac{-\Delta F}{k_B T_0} \right] \sinh \left[\frac{\alpha \sigma_0}{k_B T_0} \right] =: \mathcal{E}(\sigma, \tau_0)$$

where we have defined the function \mathcal{E} for a simpler notation in the future. Now that Equations 1.7, 1.8, 1.8 finalise the generalised model to Toda's. We are left with a numerical method for simulation.

1.5 Numerical scheme – finite volume method

To solve the system numerically, we approximate the sample by portions of volumes as Figure 1.7 and adjust the equations to the finite volume form.

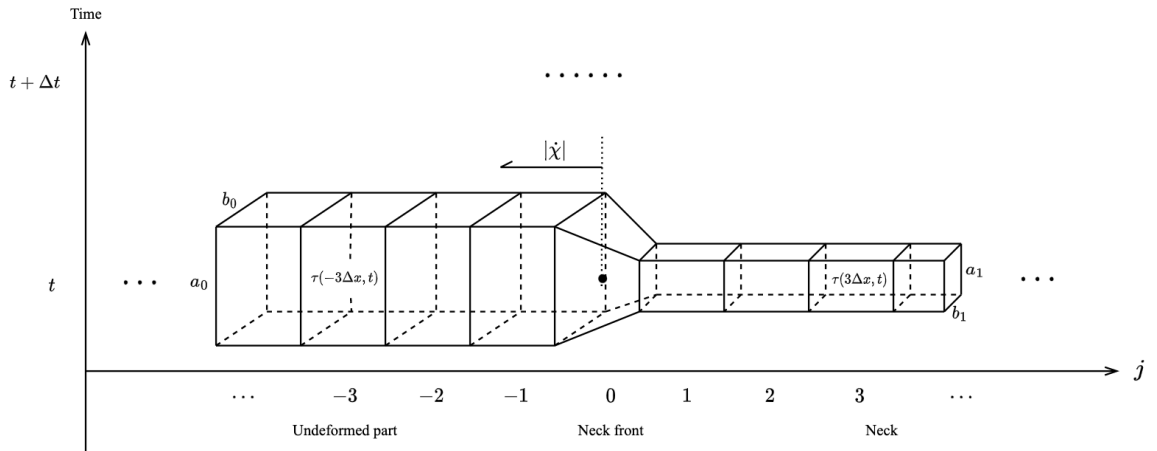


Figure 1.7: A schematic for the elements we considered in finite volume method. In simulation we will also have time step $\Delta t = 0.005s$, where for each time we have temperature of each block in the schematic recorded (so that there will be a matrix). Two temperatures at $j = -3, 3$ are for illustration purpose. Other variables will be stored in array from, determined by time t solely.

Starting from the initial condition, the variables τ, σ, ν, χ will be updated through time. Note that for τ we are updating the vector:

$$\vec{\tau}_{temp} = (\tau(-0.75), \tau(-0.75 + \Delta x), \dots, \tau(1.5 - \Delta x), \tau(1.5))^\top$$

The core of the algorithm is to develop the updating sentences. We use subscript $temp$ to denote the new value for the next time step, such variables will be determined explicitly by the current values. We define the grid scales to be $\Delta x = (2.25/4999)\text{cm}$

spatially and $\Delta t = 0.01$ s temporally. It's subtle to choose Δx , with different Δx the FVM algorithm can be delicate and care is needed in writing equations. Therefore a convergence study might be conducted, to determine the smallest spatial grid scale which doesn't affect the phase. Except this, through trying different computational domains, $[-0.75, 1.5]$, which we will use throughout the study, was enough.

For updating σ , by Equation 1.7,

$$\sigma_{temp} = \Delta t \cdot \frac{V - \mathcal{E}(\sigma, \tau_0) \left[\frac{\sigma}{E_0} \left(\lambda^2 \frac{E_0}{E_1} - 1 \right) + (\lambda - 1) \right]}{\frac{\chi}{E_0} + \lambda^2 \frac{L_0 - \chi}{E_1}} \quad (1.9)$$

For updating χ , by equation 1.4.4 and recall that χ is monotonically decreasing,

$$\chi_{temp} = \chi - \Delta t \cdot \mathcal{E}(\sigma, \tau_0) \quad (1.10)$$

For updating temperature, we will deal with the vector $\vec{\tau}$ each time. Following Figure 1.7, the heat balance equation in FVM form is:

$$\begin{aligned} & a^j b^j \rho \Delta x \frac{\tau_{temp,j} - \tau_j}{\Delta t} + a_0 b_0 \rho c_p \mathcal{E}(\sigma, \tau_0) (\tau_{temp,j} - \tau_{temp,j-1}) \\ &= -h (a^j + b^j) \tau_{temp,j} \cdot \Delta x - \left[\frac{\tau_{temp,j+1} - \tau_{temp,j}}{\Delta x} \right] \cdot \kappa_j^+ \\ & \quad + \left[\frac{\tau_{temp,j} - \tau_{temp,j-1}}{\Delta x} \right] \cdot \kappa_j^- + a_0 b_0 \eta (\lambda - 1) \mathcal{E} \sigma \delta_{0,j} \end{aligned}$$

where:

$$\begin{aligned} a^j &= \begin{cases} a_0, & j < 0 \\ (a_0 + a_1)/2, & j = 0 \\ a_1, & j > 0 \end{cases} & b^j &= \begin{cases} b_0, & j < 0 \\ (b_0 + b_1)/2, & j = 0 \\ b_1, & j > 0 \end{cases} \\ \kappa_j^+ &= \begin{cases} k_0 a_0 b_0, & j < 0 \\ k_1 a_1 b_1, & j \geq 0 \end{cases} & \kappa_j^- &= \begin{cases} k_0 a_0 b_0, & j \leq 0 \\ k_1 a_1 b_1, & j > 0 \end{cases} \end{aligned}$$

By comparison of simulation results, if we smooth the step functions above, the algorithm will be able to record more sudden changes that exceeds grid scale (happens within Δt). The smoothing function we used for above parameters is \tanh , and for $\delta_{0,j}$ is the p.d.f. to $\Phi(0, x_0^2)$. The following is an example to this technique:

$$a^j \rightarrow a_0 + \frac{a_1 - a_0}{2} \left[1 + \tanh \left(\frac{j \Delta x - 0.75}{x_0} \right) \right]$$

The value of x_0 we take is affecting the system so care must be taken. Again $x_0 = 0.005$ is the value taken after some investigation. The final updating sentence will be a tri-diagonal matrix problem

$$\text{tridiag}[\vec{A}, \vec{B}, \vec{C}] \vec{\tau}_{temp} = \vec{f} \quad (1.11)$$

$$\text{tridiag}[\vec{A}, \vec{B}, \vec{C}] = \begin{bmatrix} A(1) & C(1) & & & \\ B(2) & A(2) & C(2) & & \\ & B(3) & A(3) & C(3) & \\ & & \ddots & \ddots & \ddots \\ & & & B(n-1) & A(n-1) & C(n-1) \\ & & & & B(n) & A(n) \end{bmatrix}$$

where the entries of \vec{A} , \vec{B} , \vec{C} , and \vec{f} can be read from the FVM form heat balance equation above.

The updating sentences 1.9, 1.10, 1.11 finalise our algorithm. We are now able to compare our simulation to experimental results, specifically the stress-strain curve. The stress is σ in our algorithm, while the strain is $(100 \frac{Vt}{L_0})\%$. See Chapter 2 for the comparison with system parameters proposed half by Toda and half by Nathan. There will also be an analysis to the parameters in the next chapter.

Chapter 2

Tuning parameters

In this section we analyse the effect on the model fitting when changing parameters in Nathan's model. The parameters are allowed to fall in a certain interval rather than an exact value. The system parameters we are possible and would like to change are mentioned in the following table, with the values used in Nathan's report:

k_i (erg cm $^{-1}$ s $^{-1}$ K $^{-1}$)	E_i (g cm $^{-1}$ s $^{-2}$)	ρ (g cm $^{-3}$)	c_p (erg g $^{-1}$ K $^{-1}$)	λ
1.50×10^4	2.75×10^{10}	1.34	1.12×10^7	3.5
h_i (erg cm $^{-2}$ s $^{-1}$ K $^{-1}$)	α (cm 3)	v_0 (cm s $^{-1}$)	ΔF (erg)	η
2.33×10^3	3.39×10^{-21}	2.25×10^{72}	8.78×10^{-12}	1

Table 2.1: Adjustable parameters ($i = 0, 1$)

Note that the simulation also involves parameters directly from the experiments, where we set them to be fixed:

a_0 (cm)	b_0 (cm)	L_0 (cm)	k_B (g cm 2 s $^{-2}$ K $^{-1}$)	V (cm s $^{-1}$)	T_a (K)
0.657	0.008	6.965	1.3807×10^{-16}	1/6	293.15

Table 2.2: Fixed parameters

We will start with our replicate to parameters proposed by Nathan, shown in Table 2.1. There are majorly four problems in fitting:

- The average value of stress (centre of oscillation) is higher than experiments.
- The stress is in an increasing trend compared to experiments, in which the stress is decreasing gradually.¹

¹The final increase in stress is due the an inevitable feature of experiments, we would just focus on fitting the first half.

- The frequency is slower than experiments, as illustrated in the inset.
- The drop for each oscillation is steeper than that of the experiments.

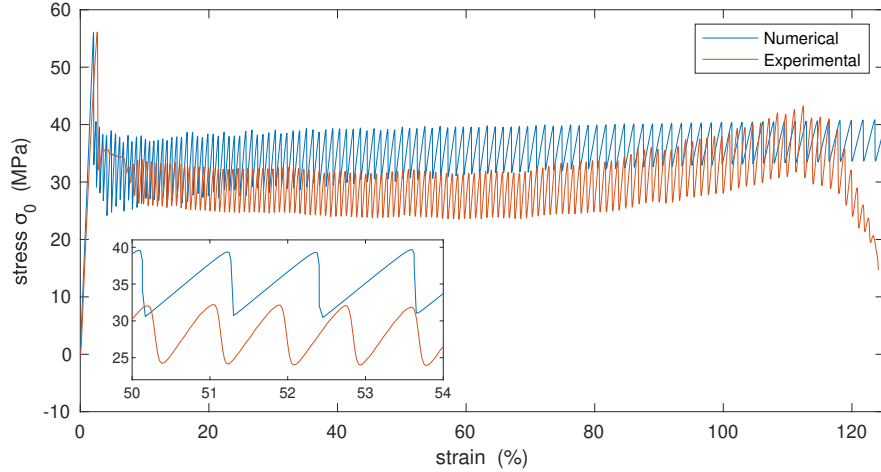


Figure 2.1: Comparison of numerical and experimental results, using the parameters proposed by Nathan.

2.1 Effects of changing individual parameters

2.1.1 Varying E_0

As E_0 is the elastic modulus of the original sample, and the fact that the sample would undergo elastic deformation, we expect the initial slope to be exactly E_0 . To fit the experiments, we take $E_0 = 2.25 \times 10^{10} \text{ g cm}^{-1} \text{ s}^{-2}$. Later by personal communication with Chaoying Wan, we should take slope of the first straight line in the region strain $\epsilon < 0.2\%$, which means around $2.5 \times 10^{10} \text{ g cm}^{-1} \text{ s}^{-2}$.

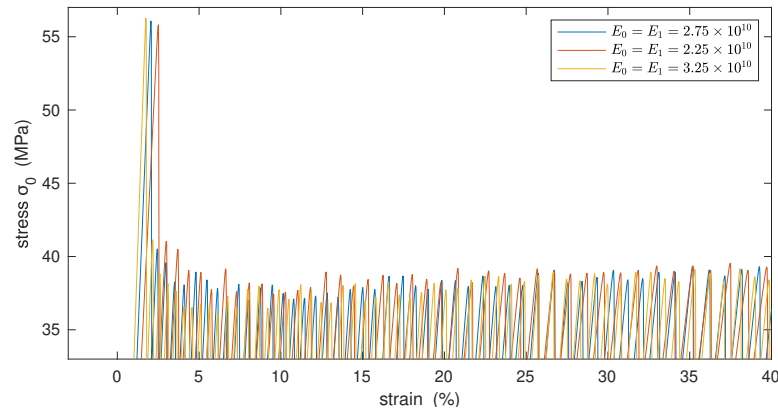


Figure 2.2: Varying E_0 , retaining the top-left.

2.1.2 Varying E_1

When a material is plastic deformed, the elastic modulus will be larger. We expect this happens to the neck similarly – the average modulus of the banding pattern will be higher. From our definition to compliance, $D(\chi; L_0) = \frac{\chi}{E_0} + \lambda^2 \frac{L_0 - \chi}{E_1}$, we know that initially $D(L_0; L_0) = L_0/E_0$ and finally $D(0; L_0) = \lambda^2 L_0/E_1$. Therefore we are free to set E_1 under the constraint $E_1 < \lambda^2 E_0$. From Figure 2.3, we see that a larger E_1 is able to suppress the increasing trend of average stress, and therefore closer to the experimental average. However, the frequency is also higher for a larger E_1 , as in the inset. We take $E_1 = 6.1 \times 10^{10} \text{ g cm}^{-1} \text{ s}^{-2}$.

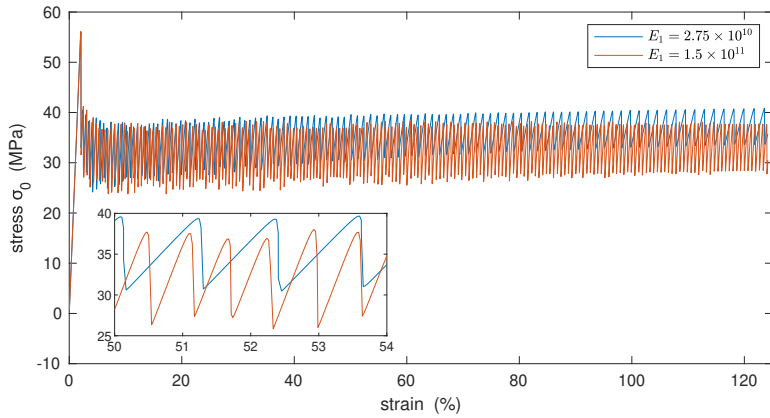


Figure 2.3: Varying E_1 , with the inset a closer look.

2.1.3 Varying ΔF

ΔF is changing the height of the entire stress curve, see Figure 2.4. Some extreme values would also change some properties of the oscillation, we omit them here.

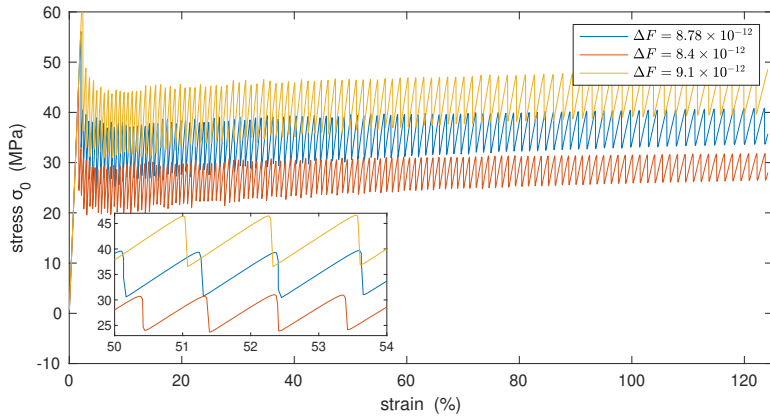


Figure 2.4: Varying ΔF , with the inset a closer look.

2.1.4 Varying α

Adjusting α changes the height of the whole curve in the opposite direction, similar to that of ΔF . They both appear in Eyring's equation, while in different functions $\exp(\cdot)$ and $\sinh(\cdot)$. So indeed they provide similar affects. And due to the difference, a combination of these two might be considered, see Section 2.2.1.

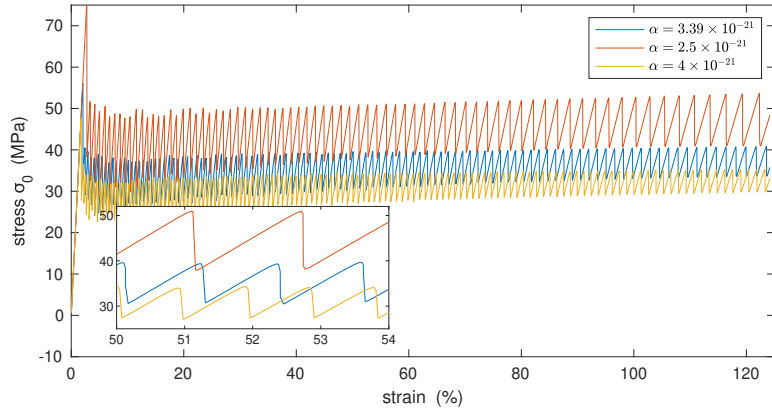


Figure 2.5: Varying α , giving similar effect as ΔF .

2.1.5 Varying ρ

The initial density of the sample can be directly measured. But due to the age of the experiments, there might be minor changes in the samples preserved. We take $\rho = 1.38 \text{ g cm}^{-3}$. Despite this, it's still worth looking at the effect it brings. As Figure 2.6, larger ρ corresponds to a higher average stress and frequency, vice versa. The inset box demonstrates this in detail. There's no change in the height of the yield point.

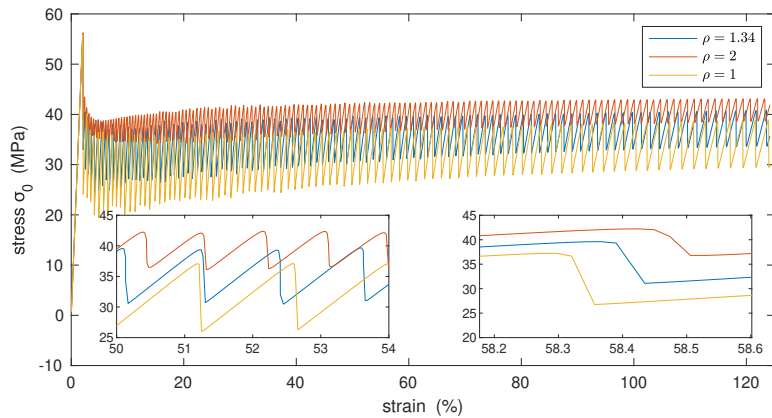


Figure 2.6: Varying ρ , with the inset a closer look.

This inspires us that if we restore the smaller density ρ_1 for the deformed region, then there's a chance to replicate the gradual decrease in average stress as the experiment. We'll discuss this modification in details later in Chapter 3.

2.1.6 Varying k_i

Varying k_0 and k_1 simultaneously affects the phase and slightly the amplitude, as shown in Figure 2.7.

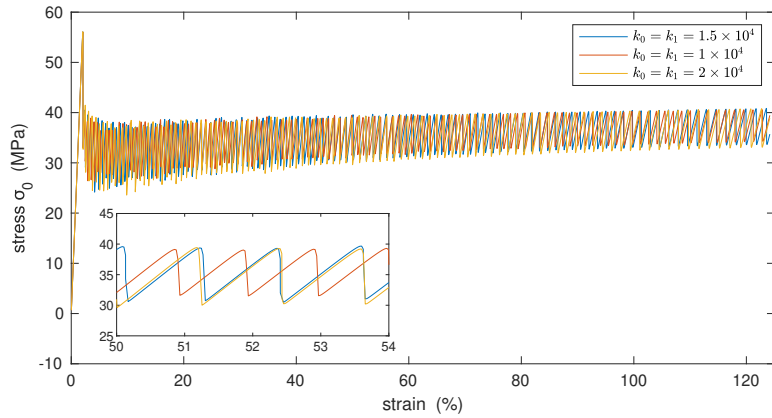


Figure 2.7: Varying k_0 and k_1 simultaneously.

It occurs to us that although having fairly tiny effects on stress, varying k_0 and k_1 simultaneously may bring more significant changes to the temperature. We therefore look at the temperature profile against time. It turns out that besides the phase change, the temperature loss of the hotter region (neck) seems to be faster for larger k_i . The temperatures for neck front don't change much, we omit them here.

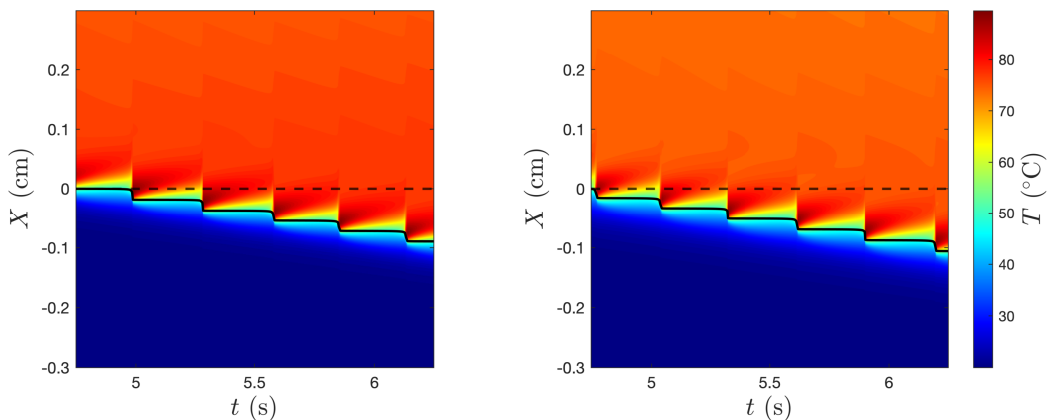


Figure 2.8: Temperature intensity plot with **Left:** $k_0 = k_1 = 1.5 \times 10^4 \text{ erg cm}^{-1} \text{ s}^{-1} \text{ K}^{-1}$, and **Right:** $k_0 = k_1 = 2 \times 10^4 \text{ erg cm}^{-1} \text{ s}^{-1} \text{ K}^{-1}$.

There will be more changes in stress-strain relation if we set both k_0 and k_1 to different values. To illustrate this, we fix k_0 while change k_1 to achieve different ratios. With a larger ratio, the amplitude is larger, along with a lower frequency. We take them to be $k_0 = 1.5 \times 10^4 \text{ erg cm}^{-1} \text{ s}^{-1} \text{ K}^{-1}$ and $k_1 = 3.7 \times 10^4 \text{ erg cm}^{-1} \text{ s}^{-1} \text{ K}^{-1}$ respectively.

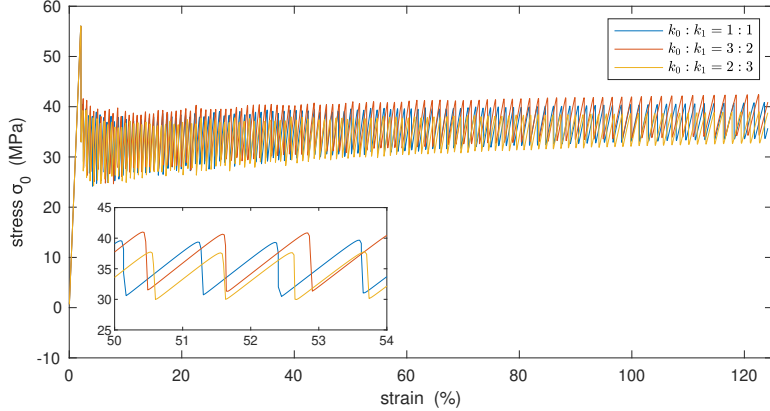


Figure 2.9: Different k_0 and k_1 , retaining k_0 while controlling the ratio.

2.1.7 Varying v_0

An increase in v_0 corresponds to an decrease in the stress, and vice versa. However, the change is not sensitive to v_0 , compared to ΔF and α . The reason might be that ΔF and α are in the exponential term ($\nu \simeq 2v_0 \exp[-\frac{\Delta F}{k_B T_0}] \exp[\frac{\alpha \sigma_0}{k_B T_0}]$), while v_0 is a factor in front of them.

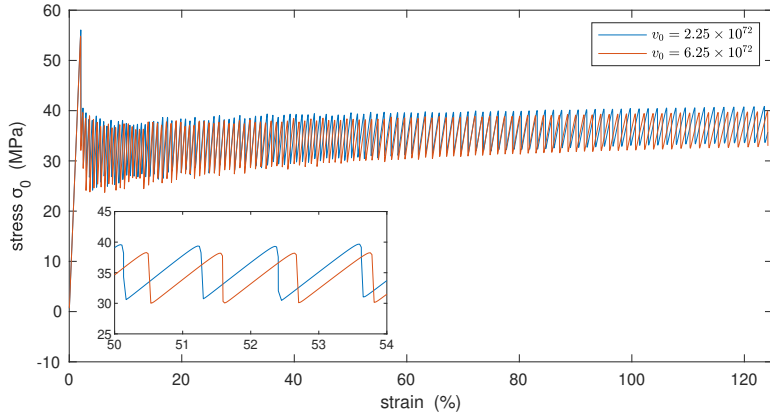


Figure 2.10: Varying v_0 causes lift in the stress curve.

Similar thermal plots as the previous subsection also shows no significant relation to the change of v_0 , we omit them here. Following the value proposed by Toda, we use $v_0 = 2.25 \times 10^{72} \text{ cm s}^{-1}$.

2.1.8 Varying c_p

Varying c_p won't affect the height of the yield point. While there will be changes in the average stress, frequency, and amplitude. Another prominent relation is that with a large specific heat capacity, the speed of plastic deformation is also quicker, see the slope of drops in the inset on the right. The change is quite sensitive here.

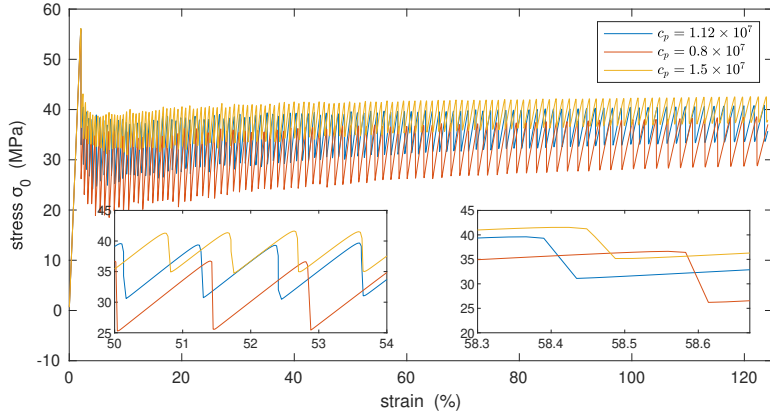


Figure 2.11: Varying c_p .

We shall also look at the effect on temperature intensity. Figure 2.12 shows that the temperature is generally lower for smaller heat capacity, and also the temperature change from the neck front to the undeformed region is more gradual (though not so obvious).

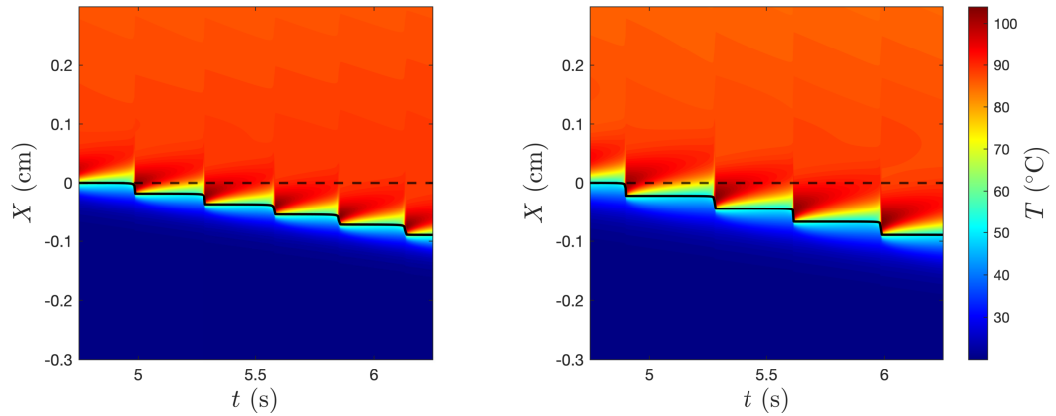


Figure 2.12: Temperature intensity plot with **Left:** $c_p = 1.12 \times 10^7 \text{ erg g}^{-1} \text{ K}^{-1}$, and **Right:** $c_p = 0.8 \times 10^7 \text{ erg g}^{-1} \text{ K}^{-1}$.

We can also examine the temperature at neck front, the comparison is shown in Figure 2.13.

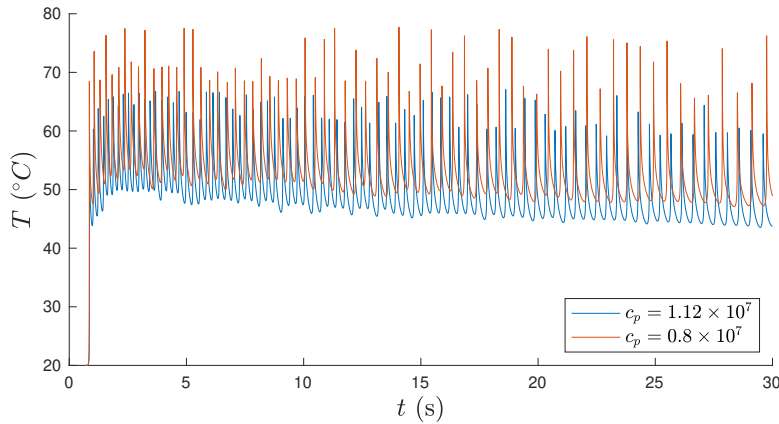


Figure 2.13: Approximated temperature at neck front against time. Comparing two different heat capacities.

It's as our expectation that for larger heat capacity, the temperature is lower, as the blue curve indicates. The oscillation for $c_p = 0.8 \times 10^7$ seems to be fiercer, with a higher peak (red curve). Thus for parameter c_p we can also refer to the temperature at neck front if experimental data is available. We set $c_p = 1.04 \times 10^7 \text{ erg g}^{-1} \text{ K}^{-1}$.

2.1.9 Varying h_i

By varying the heat dissipation rate h_i by an order of ten, we are able to see changes in amplitude. However, the variation seems to be small, relative to the magnitude of change.

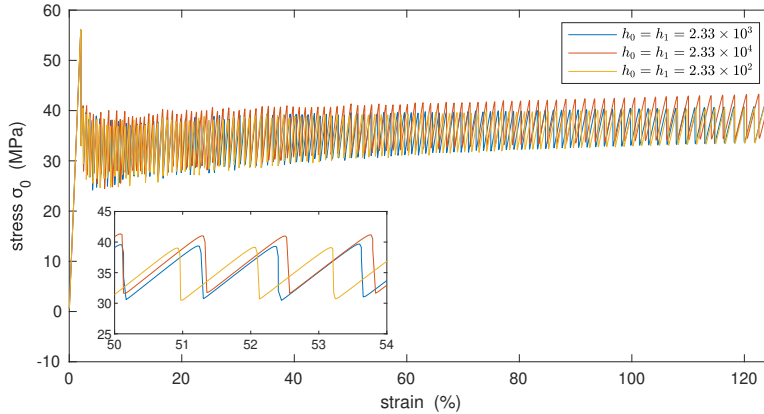


Figure 2.14: Varying h_0 and h_1 simultaneously.

In terms of varying ratio, similarly we fix $h_0 = 2.33 \times 10^3$. There is little change as well, except phase changes. With a huge change while small effect in tuning, we'll simply take the value $h_0 = h_1 = 2.33 \times 10^3 (\text{erg cm}^{-2} \text{ s}^{-1} \text{ K}^{-1})$.

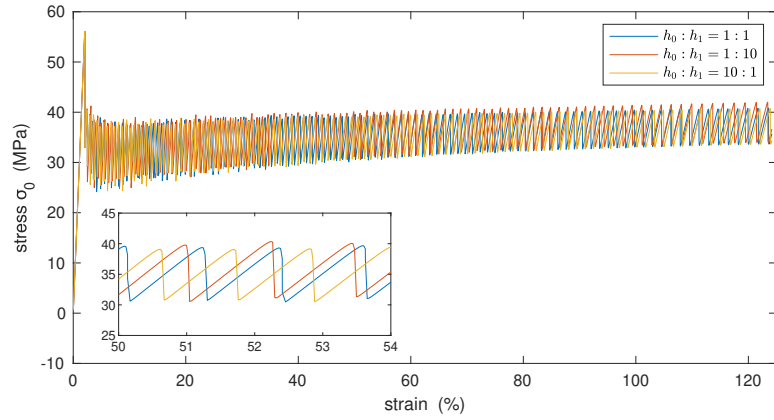


Figure 2.15: Fixing h_0 , while varying the ratio of h_0 and h_1 .

Again we feel obliged to look at the change in temperature intensity it brings. Figure 2.16 is the thermal map for this. Finally there are observations.

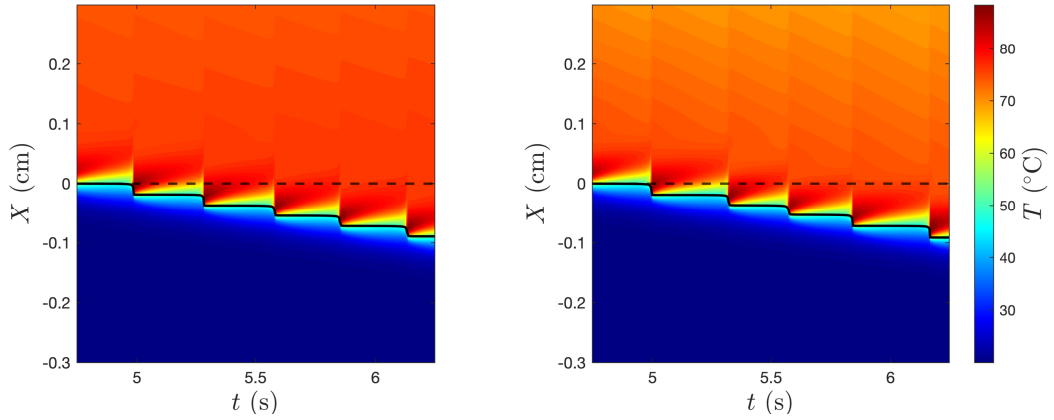


Figure 2.16: Temperature intensity plot with **Left:** $h_0 = h_1 = 2.33 \times 10^3 \text{ erg cm}^{-2} \text{ s}^{-1} \text{ K}^{-1}$, and **Right:** $h_0 = h_1 = 8.33 \times 10^3 \text{ erg cm}^{-2} \text{ s}^{-1} \text{ K}^{-1}$.

With a larger h_i , the temperature at neck is generally lower, along with a larger fluctuation. If experimental data is available, our choice to the set of values may be changed. As for the neck front, Figure 2.17 gives a specific view. There wasn't many differences, compared to looking at the neck close to the end.

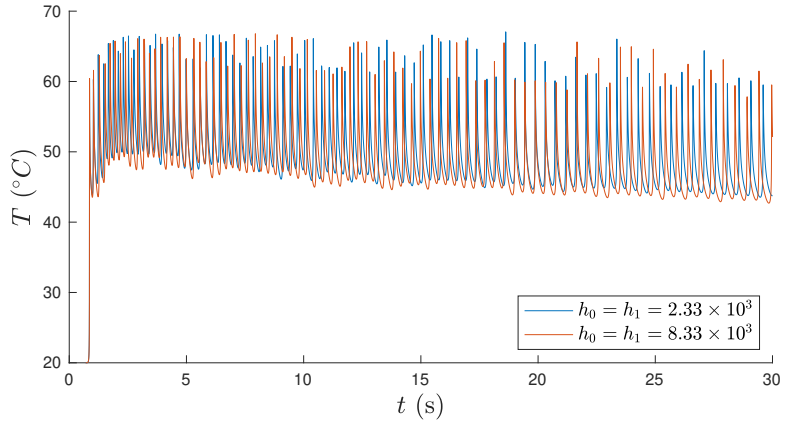


Figure 2.17: Temperature at neck front against time. Comparing two different sets of heat loss rate from sample to air.

2.1.10 Varying λ

Recall that the draw ratio λ is defined by $\frac{\rho_0 S_0}{\rho_1 S_1}$. Thus it can be directly determined by measuring the sample. However, due to the irregular shape of sample after stretch, practically we measure initial length L_0 , initial cross-sectional area S_0 , final length of undeformed and deformed region (without any elastic stretch) l_0^* , l_1^* . With this measurements $\lambda = \frac{l_1^*}{L_0 - l_0^*}$. There might be uncertainties in measuring, so that small adjustments on λ are still desirable. In our model, λ has huge effect on frequency, stress amplitude, or even oscillation properties. This is probably the most sensitive parameter, so experimental data about this will be really helpful.

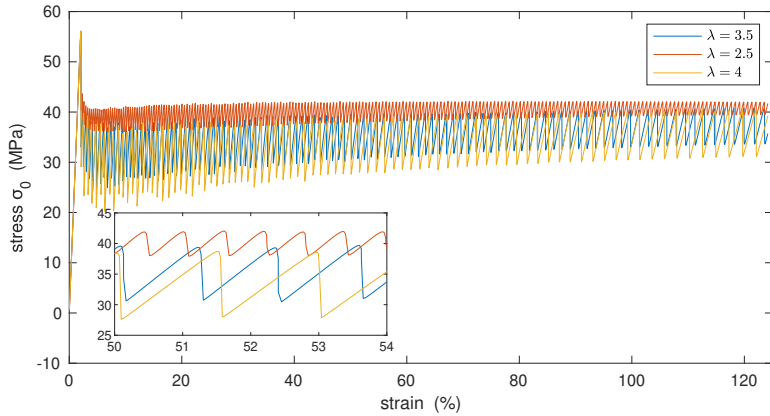


Figure 2.18: Varying λ , The case $\lambda = 2$ was the value Toda used where consequently the speed of neck propagation $|\dot{\chi}|$ equals the speed of plastic deformation ν .

2.1.11 Varying η

It is mentioned by Toda that all the work done are converted into heat when drawing a PET sample [4], which implies $\eta = 1$. Figure 2.19 shows the effect different values bring.

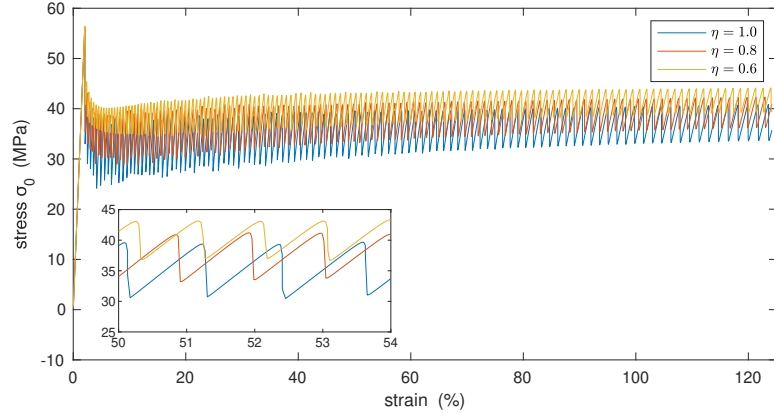


Figure 2.19: Varying η .

Since η is efficiency parameter for heat conversion, there might be changes in temperature. The simulation results (Figure 2.20) shows that there are changes to the temperature flow near neck front, towards the deformed parts; One can see the fading pattern of low temperature (yellow) for low conversion efficiency. At neck front, as expected, with less heat supply from mechanical work the temperature is lower, shown as Figure 2.21. For extreme values like 0.6, both the temperature plot and the stress-strain curve seems to be abnormally smooth in shape, which might not be accepted in our modelling.

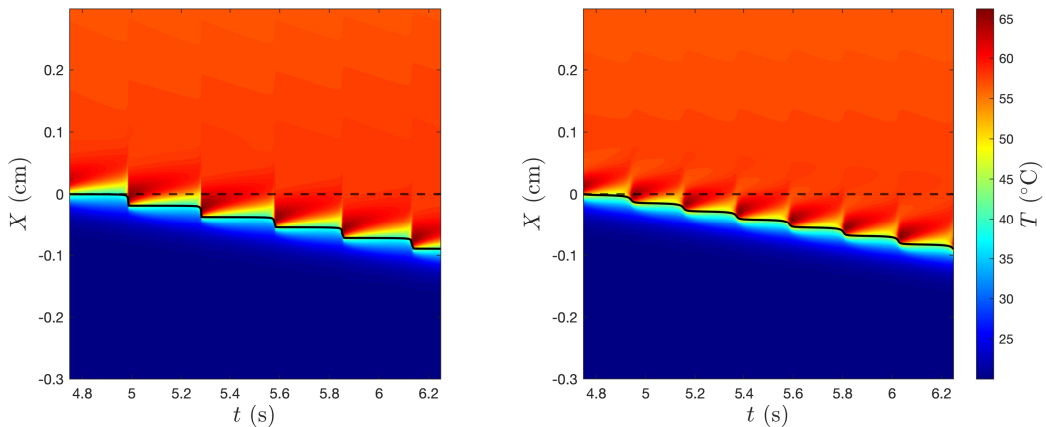


Figure 2.20: Temperature intensity plot with **Left:** $\eta = 1.0$, and **Right:** $\eta = 0.6$.

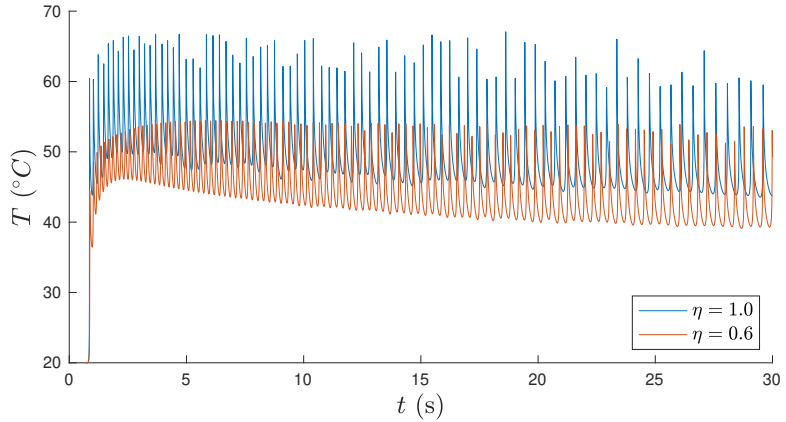


Figure 2.21: Temperature at neck front against time. Comparing two different conversion efficiency from mechanical work to heat.

2.2 Further suggestions on fitting parameters

2.2.1 Combining ΔF and α

As mentioned in Section 2.1.4, a combination of change in ΔF and α can be considered. With a smaller α and the corresponding ΔF fitted, the height is lower. This is one of the most important techniques if we want to adjust the average stress for oscillation. We take $(\Delta F, \alpha) = (8.55 \times 10^{-12}, 2.95 \times 10^{-21})$.

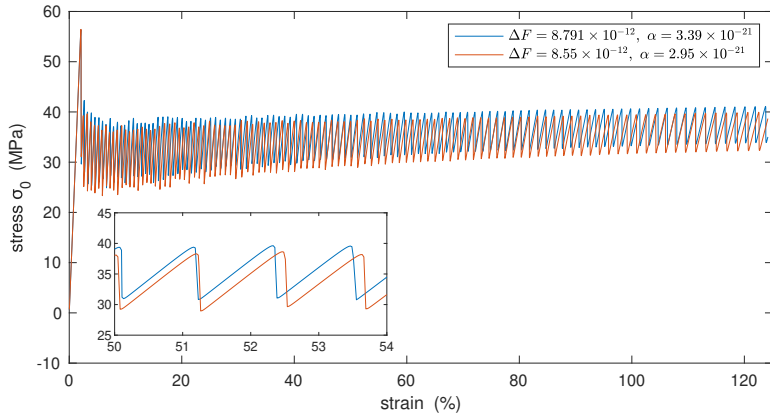


Figure 2.22: Comparison of two sets of values for ΔF and α . The yield point is preserved while the average stress can be adjusted.

2.2.2 Sensitivities of parameters and fitting

In this subsection we make a summary of sensitivity of parameters, and consequently to which experimental results should we compare. The following list is a summary. Unless otherwise stated, the parameters are fitted according to the stress-strain curve.

- ρ and λ should be directly measured from experiments, they are the uppermost sensitive and important parameters to the system. For λ one should follow the computation method proposed in Section 2.1.10, measuring directly by the definition might be easier, but the shape of sample can be irregular and leads to great uncertainty.
- c_p is also one of the most sensitive parameters. If possible, it would be helpful to determine the value before the experiments starts. One can also compare to the temperature at neck front if that's feasible.
- E_1 has considerate sensitivity, with a big range of reasonable values. It helps to have a tiny stretch experiment for the neck to get a precise value. E_0 can be directly obtained from the initial slope, which might be the most certain parameter in value.
- α and ΔF can hardly be measured. One can start from $\alpha = 3.39 \times 10^{-21}$ proposed by Toda and fit ΔF to the height of yield point. After that close to the end, a couple of value can be tried to fit the average stress, using the technique in the previous subsection.
- v_0 might be the most insensitive parameter, my suggestion is to retain Toda's value 2.25×10^{72} . η brings change, but it's experimentally confirmed [4] it should be close to 1. If it's not the case, then η is quite sensitive, and can be fitted both in the view of stress-strain and thermal map.
- The ratio of k_0 and k_1 should be considered, which is useful to adjust the frequency. The ratio is sensitive, though not much. Besides, the thermal map is sensitive to the magnitude of k_i . Therefore we can first fit the magnitude of k_0 according to thermal maps, and then determine k_1 by fitting the ratio.
- The only way to fit h_0 and h_1 seems to compare to the temperature map if possible, otherwise we can retain the value 2.33×10^3 . They are the most insensitive parameters in terms of stress-strain curve.

2.3 Simulation results and discussion

With the parameters mentioned (have been summarised in the following two tables), we present the simulation results in Figure 2.23.

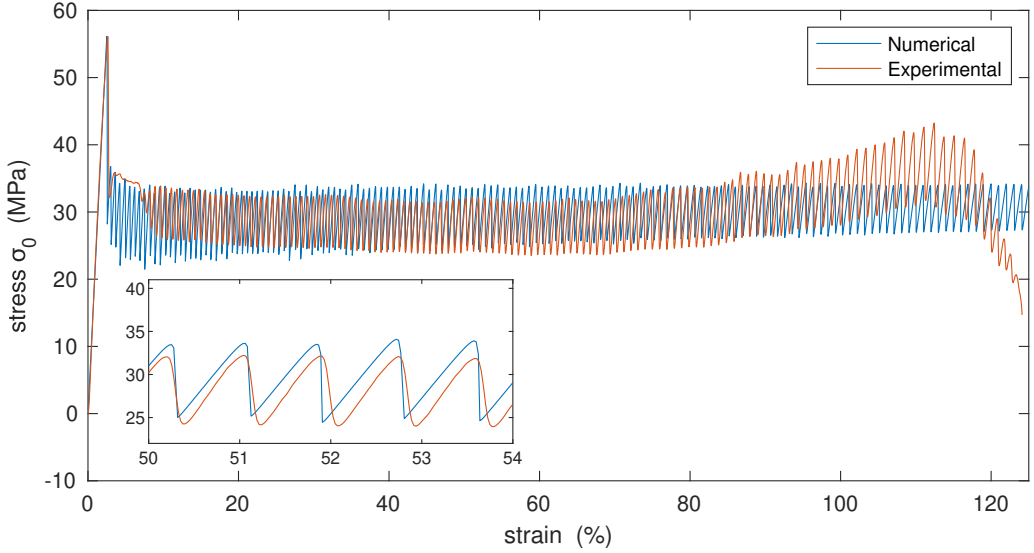


Figure 2.23: Simulation results with the proposed parameters in Chapter 1.

$k_0 \text{ (erg cm}^{-1} \text{s}^{-1} \text{K}^{-1}\text{)}$	$k_1 \text{ (erg cm}^{-1} \text{s}^{-1} \text{K}^{-1}\text{)}$	$E_0 \text{ (g cm}^{-1} \text{s}^{-2}\text{)}$	$E_1 \text{ (g cm}^{-1} \text{s}^{-2}\text{)}$
1.50×10^4	3.70×10^4	2.25×10^{10}	6.1×10^{10}
$h_i \text{ (erg cm}^{-2} \text{s}^{-1} \text{K}^{-1}\text{)}$	$v_0 \text{ (cm s}^{-1}\text{)}$	$\alpha \text{ (cm}^3\text{)}$	$\Delta F \text{ (erg)}$
2.33×10^3	2.25×10^{72}	2.95×10^{-21}	8.55×10^{-12}
$\rho \text{ (g cm}^{-1}\text{)}$	$c_p \text{ (erg g}^{-1} \text{K}^{-1}\text{)}$	λ	η
1.38	1.04×10^7	3.5	1

Table 2.3: Summary of parameters mentioned in Section 4.1 and taken to produce the above comparison.

$a_0 \text{ (cm)}$	$b_0 \text{ (cm)}$	$L_0 \text{ (cm)}$	$V \text{ (cm s}^{-1}\text{)}$
0.657	0.008	6.965	1/6

Table 2.4: Summary of other parameters that do not need to be fitted.

The amplitude and frequency are well fitted. But some problem about fitting persists:

- We know by assigning E_1 a sufficiently large value, we can make the stress oscillation inclined downwards. However, with such a large E_1 , it's hard to fit the frequency and height; Moreover, it's unrealistic since $D(\chi; L_0) = \frac{\chi}{E_0} + \frac{L_0 - \chi}{E_1}$ will then vary only in a very small range, or even decrease as the neck propagates. We tried to achieve a balance and took 6.1×10^{10} here.
- The drop in stress for each oscillation is sharper than the experiments. This can be adjusted by c_p as our analysis but the improvement is small.

- The initial stress (at strain from 5% to 10%) in our simulation undergo an oscillation with a large amplitude, unlike the relatively smooth descent (delayed oscillation) in experiments.
- The frequency of oscillation actually varies for different stages in strain. Therefore it's hard to fit for any places in the graph.

The biggest problem with our model other than fitting is that the property of oscillation is not sensitive to the initial length, unlike the sensitivity we obtained from the experiments (see table below). In the future it might help to control the sample width and thickness, and have a rigorous look at the qualitative effect brought by initial length L_0 .

a_0 (cm)	b_0 (cm)	L_0 (cm)	Is there stress oscillation? ($V = 1/6$ cm s $^{-1}$)
0.603	0.008	7.258	NO
0.702	0.008	7.217	NO
0.648	0.007	7.142	NO
0.657	0.008	6.965	YES
0.549	0.08	6.963	NO

Table 2.5: Qualitative results of experiments conducted.

One case of this is that when fitting the parameter, one should not aim at fitting the curve exactly, but fitting the ability for the model to reflect the sensitivity on L_0 . However, this is hard since this might implies choosing extreme parameters.

Chapter 3

Introducing density change

Arguably, the most restrictive assumption in Nathan's model is the conservation of volume. That is, we are assuming the undeformed and the deformed region are of the same density. According to F. Ronkay and T. Czigány [2], during stress oscillation the density ρ_1 of neck can differ significantly to the density ρ_0 of the undeformed region. In this section we will release this assumption and change the density ρ in system parameters to ρ_0 and ρ_1 for undeformed and deformed respectively.

We expect ρ_1 to be smaller than ρ_0 . Experimentally, the banding pattern observed at the neck is due to cavitation, where the porosity can reach up to 50%. Therefore it is reasonable to assume $\rho_1 < \rho_0$. Another intuitive explanation is, a smaller density implies smaller average stress, illustrated as Figure 2.6 in the previous section. Hence we guess a smaller ρ_1 will cause decrease in average stress, and therefore fit the experiment better.

3.1 Re-derivation of governing equations

We start with the new **stress-strain relation**. By conservation of mass, we have:

$$\rho_0 S_0 L_0 = \rho_0 S_0 \chi + \rho_1 S_1 (L - \chi),$$

Following the definition of draw ratio, $\lambda := \rho_0 S_0 / \rho_1 S_1$, dividing $\rho_1 S_1$ both sides and collect terms:

$$L - \chi = \lambda (L_0 - \chi)$$

Note that this is exactly the same equation as derived by Nathan. Hence the expressions for l_0 and l_1 are unchanged, and thus V :

$$l_0 = \chi \left(\frac{\sigma_0}{E_0} + 1 \right), \quad l_1 = \lambda (L_0 - \chi) \left(\frac{\sigma_1}{E_1} + 1 \right)$$

$$V = \dot{\chi} \left\{ \frac{\sigma_0}{E_0} - \lambda \frac{\sigma_1}{E_1} + (1 - \lambda) \right\} + \chi \frac{\dot{\sigma}_0}{E_0} + \lambda (L_0 - \chi) \frac{\dot{\sigma}_1}{E_1}$$

We can eliminate σ_1 by $F = S_0\sigma_0 = S_1\sigma_1$ from equilibrium, and by using the fact that $|\dot{\chi}| = -\dot{\chi}$, we can reproduce a similar expression for $\dot{\sigma}_0$ as Nathan did:

$$\begin{aligned} \implies V &= \dot{\chi} \left\{ \frac{\sigma_0}{E_0} - \lambda \frac{S_0}{S_1} \frac{\sigma_0}{E_1} + (1 - \lambda) \right\} + \chi \frac{\dot{\sigma}_0}{E_0} + \lambda (L_0 - \chi) \frac{S_0}{S_1} \frac{\dot{\sigma}_0}{E_1} \\ \implies V &= |\dot{\chi}| \left\{ \frac{\sigma_0}{E_0} \left(\lambda \frac{S_0}{S_1} \frac{E_0}{E_1} - 1 \right) + (\lambda - 1) \right\} + \dot{\sigma}_0 \left(\frac{\chi}{E_0} + \lambda^2 \frac{\rho_1}{\rho_0} \frac{L_0 - \chi}{E_1} \right) \\ \implies \dot{\sigma}_0 &= \frac{1}{D(\chi; L_0)} \left\{ V - |\dot{\chi}| \left[\frac{\sigma_0}{E_0} \left(\lambda^2 \frac{\rho_1}{\rho_0} \frac{E_0}{E_1} - 1 \right) + (\lambda - 1) \right] \right\} \end{aligned} \quad (3.1)$$

where we define $D(\chi; L_0) := \frac{\chi}{E_0} + \lambda^2 \frac{\rho_1}{\rho_0} \frac{L_0 - \chi}{E_1}$ as the system elastic compliance in this new model. Note that the difference to the previous expression is the ratio of two densities. From now on we abbreviate σ_0 by σ as we did in Chapter 1.

In terms of the **heat balance equation**, now the parameter ρ becomes a function $\rho(x) := \rho_0 H(-x) + \rho_1 H(x)$, where as usual $H(x)$ is the Heaviside function. Similarly we consider the mass conservation over a short time period Δt to derive the advection term:

$$\begin{aligned} \implies \rho_0 S_0 |\dot{\chi}| \Delta t &= \rho_1 S_1 |\dot{\chi}| \Delta t + \rho_1 S_1 \nu \Delta t \\ \implies (\lambda - 1) |\dot{\chi}| &= \nu \\ \implies \text{advection speed} &= \begin{cases} |\dot{\chi}|, & x < 0 \\ |\dot{\chi}| + \nu, & x > 0 \end{cases} = (1 + H(x)(\lambda - 1)) |\dot{\chi}| \end{aligned} \quad (*)$$

which is again the same as the speed we previously derived. Therefore we have the expression for heat balance equation, with the difference in ρ being a function:

$$\begin{aligned} S(x) \rho(x) c_p \left(\frac{\partial T}{\partial t} + (1 + H(x)(\lambda - 1)) |\dot{\chi}| \frac{\partial T}{\partial x} \right) \\ = -r(x) (T - T_a) + \frac{\partial}{\partial x} \left(\kappa(x) \frac{\partial T}{\partial x} \right) + S_0 \eta (\lambda - 1) |\dot{\chi}| \sigma \delta(x) \end{aligned} \quad (3.2)$$

Finally, according to $(*)$, the appearance of ρ_1 is not changing **Eyring's equation**:

$$|\dot{\chi}| = \frac{\nu}{\lambda - 1} = \frac{2v_0}{\lambda - 1} \exp \left[\frac{-\Delta F}{k_B T_0} \right] \sinh \left[\frac{\alpha \sigma}{k_B T_0} \right] =: \mathcal{E}(\sigma, \tau_0) \quad (3.3)$$

3.2 Numerical scheme of the new model

Again we use the finite volume method with smoothed parameters to provide a direct simulation of the new model. We start with parameters with jumps for simplicity

and we'll replace them by smooth approximation functions later. Divide the time into time step with gap $\Delta t = 0.01s$, and spatial step with gap $\Delta x = \frac{1.5 - (-0.75)}{5000 - 1}$. Again in our context, we denote the updated variable by the subscript $temp$.

For updating σ , by (3.1),

$$\sigma_{temp} = \Delta t \cdot \frac{V - \mathcal{E}(\sigma, \tau_0) \left[\frac{\sigma}{E_0} \left(\lambda^2 \frac{\rho_1}{\rho_0} \frac{E_0}{E_1} - 1 \right) + (\lambda - 1) \right]}{\frac{\chi}{E_0} + \lambda^2 \frac{\rho_1}{\rho_0} \frac{L_0 - \chi}{E_1}} \quad (3.4)$$

For updating χ , by (3.3) and by noting that χ is monotonically decreasing, we deduce that the updating sentence has no change:

$$\chi_{temp} = \chi - \Delta t \cdot \mathcal{E}(\sigma, \tau_0) \quad (3.5)$$

For updating $\vec{\tau}$, it's all about the changed FVM approximation of the heat balance equation. Drawing (3.2),

$$\begin{aligned} S(x)\rho(x)c_p & \left(\underbrace{\frac{\partial \tau}{\partial t}}_1 + \underbrace{(1 + H(x)(\lambda - 1))|\dot{\chi}| \frac{\partial \tau}{\partial x}}_2 \right) \\ &= -r(x)\tau + \frac{\partial}{\partial x} \left(\kappa(x) \frac{\partial T}{\partial x} \right) + S_0\eta(\lambda - 1)|\dot{\chi}|\sigma\delta(x) \end{aligned}$$

Only the left hand side involves the density function $\rho(x)$, therefore we retain other terms and focus on 1 and 2.

Term 1:

$$\begin{aligned} S(x)\rho(x)c_p \frac{\partial T}{\partial t} & \longrightarrow a^j b^j \rho^j c_p \Delta x \frac{\partial \tau}{\partial t} \\ & \approx a^j b^j \rho^j \Delta x \frac{\tau_{temp,j} - \tau_j}{\Delta t} \end{aligned}$$

Term 2:

$$\begin{aligned} S(x)\rho(x)c_p (1 + H(x)(\lambda - 1))|\dot{\chi}| \frac{\partial \tau}{\partial x} & \longrightarrow a_0 b_0 \rho_0 c_p |\dot{\chi}| \frac{\partial \tau}{\partial x} \Delta x \\ & \approx a_0 b_0 \rho_0 c_p \mathcal{E}(\sigma, \tau_0) (\tau_{temp,j} - \tau_{temp,j-1}) \end{aligned}$$

So that the change on density $\rho(x)$ only affects **Term 1**. As previously, updating the temperature profile $\vec{\tau}$ is equivalent to solve the tri-diagonal matrix problem

$$tridiag[\vec{A}, \vec{B}, \vec{C}] \vec{\tau}_{temp} = \vec{f} \quad (3.6)$$

After some calculation and tidying, we know that changes only arise in \vec{A} and \vec{f} .

Finally, we smooth our density function as we did on other parameters,

$$\rho(x) = \rho_0 H(-x) + \rho_1 H(x) \quad \rightarrow \quad \rho_0 + \frac{\rho_1 - \rho_0}{2} \left[1 + \tanh \left(\frac{x}{x_0} \right) \right]$$

With the above changes, the setting of our new smoothing parameter FVM method is finalised. The fitting of parameters and a comparison to experimental data will be shown in the next section.

3.3 Effect of the second density

The effect of introducing density change is beyond expectation – it's not the case that the stress gradually decays, actually the whole average stress in oscillation is lower when we have the second smaller density. What's more, the frequency is faster if we assume the neck density is lower, which again obeys our findings in Chapter 2.

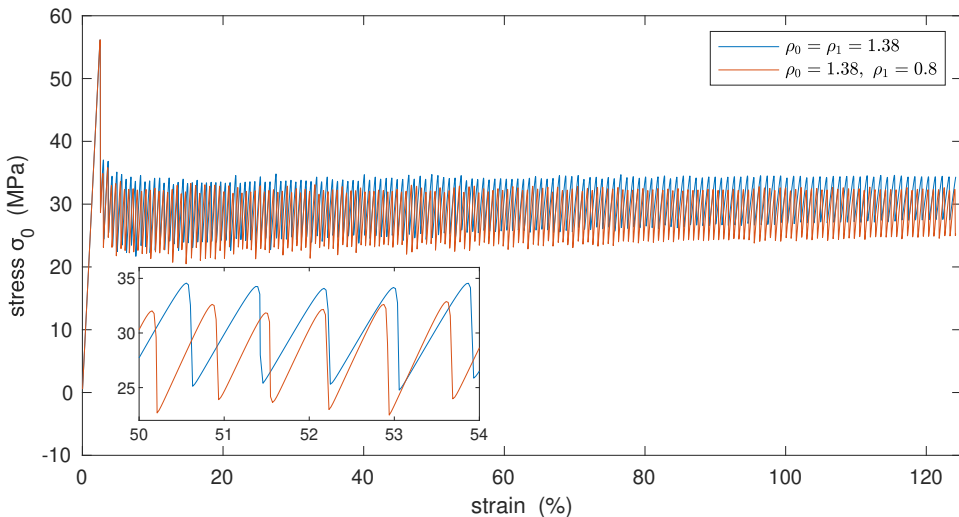


Figure 3.1: A comparison of the effect of bringing in the second density, assuming $\rho_1 = 0.8 \text{ cm s}^{-1}$.

In a good way, the model provides us a new way to adjust the average stress, on the basis of balancing ΔF and α . And the amplitude at the beginning of the oscillation (around strain = 3 ~ 8%) is suppressed, which improves one of our bullet point problems in Chapter 2. Furthermore, if one allows ρ_0 to be higher than usual, the amplitude at the beginning of oscillation can be even further suppressed; Figure ?? illustrates this with a closer look in the inset.

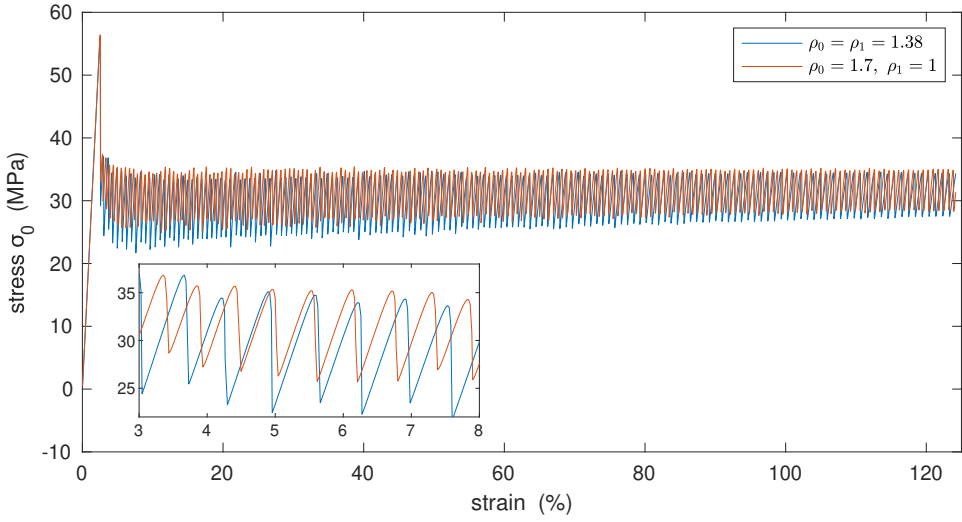


Figure 3.2: With two densities, setting unusually high value for ρ_0 can suppress the oscillation at the beginning.

Due to time limitation of the project, in my point of view the effect of second density hasn't been fully discovered. This would require more attempts and some particular experiments summarised in Chapter 4. The following is one of the fitting results, which may looks even worse than the previous model, but is lower in average stress.

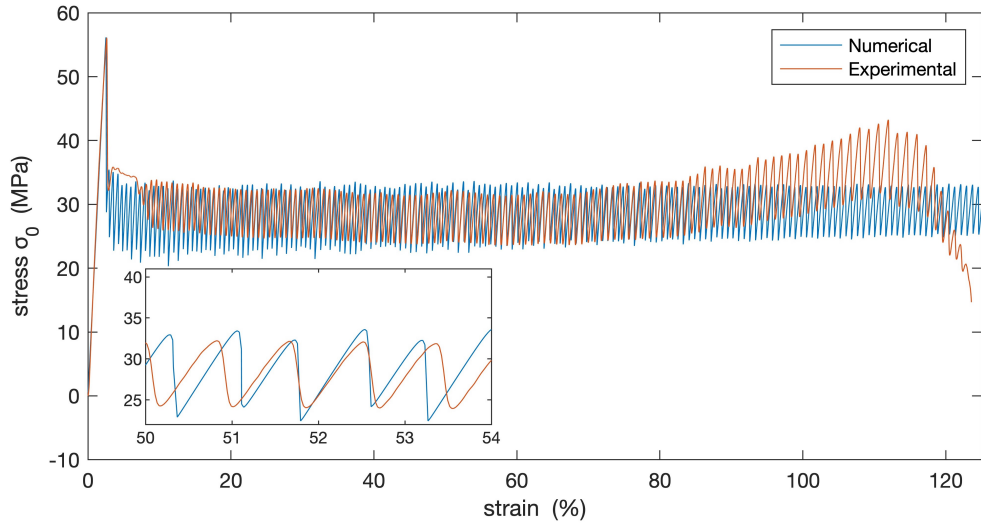


Figure 3.3: Simulation with parameter from Chapter 2, adding the second density $\rho_1 = 0.9 \text{ g cm}^{-1}$.

3.4 Comparison with the experiments

The universality of a model is an important aspect. We should fit not only the 0.5 wt % rGO sample, but also other samples with experimental data [7] on hand (PET,

0.1 wt % rGO, 0.3 wt % rGO). The stress-strain curves we obtained for different materials according to the experiments is illustrated in Figure 3.4.

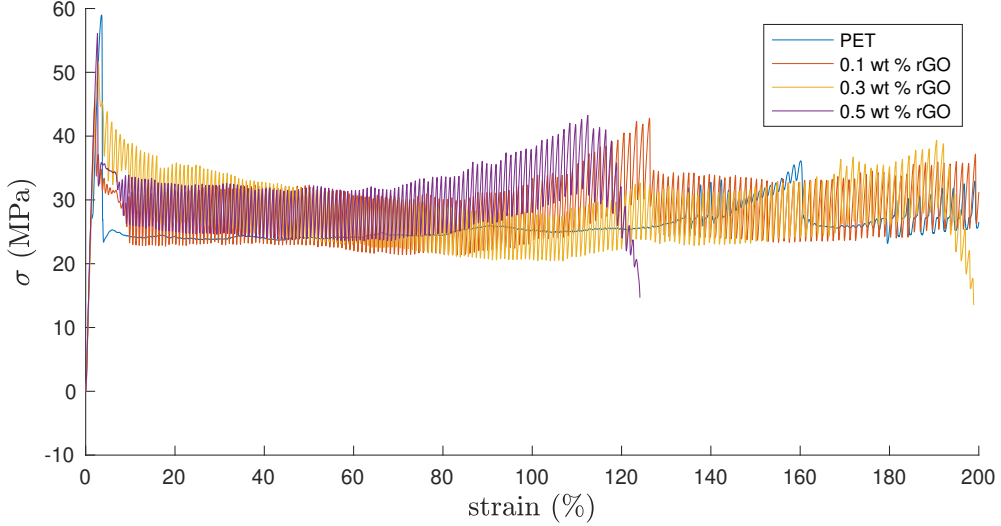


Figure 3.4: Stress-Strain curves of different materials, omitting strain $> 200\%$. Again this is because we are only interested in the parts before the rise in stress and that's strain $< 200\%$.

We observe that the average stress of oscillation for rGOs are similar, around 27 MPa; While the yield point are comparatively quite different. So primarily we expect larger differences in ΔF , α . The PET sample with no stress oscillation is qualitatively different to others, thus we expect there's a certain or a combination of parameters determining this in our model. It's also mentioned by Torrisi, et al. [6] that the mechanical and optical properties are determined by the rGO nanoparticles sensitively. So even if the concentrations are pretty close to each other, we still have room for adjustments. Due to time limitation, this can also be a continuation in the future.

Chapter 4

Conclusion

The project is continuing the generalised Toda's model, seeking refinements in the hope to predict the stress-strain curve and the critical compliance precisely. In the report we first have a background introduction to the problem and then derivation and summary of the two models in history, the Barenblatt's model and the Toda's model. After that we derived the generalised Toda's model proposed by Nathan together with its computational schemes.

Taking on the background, we analysed the parameters related in the generalised Toda's model. We then found out the way to adjust average stress without changing the yield point, and the way to make oscillation inclined decreasingly. We also observed that the ratio $k_0 : k_1$ matters, and h_0, h_1 affects little on the stress-strain but much more on the thermal map. In the end we summarised the parameter sensitivity and gave suggestions for further fitting. In Chapter 3 we introduced density difference for the neck and the undeformed part, which is the most restrictive assumption in Nathan's model. We then see the adaption gives another way to adjust the average stress and to suppress amplitude at the beginning of oscillation. However, the advantage of this hasn't been fully discovered.

The next step might be to discover more about the following, or following the two-stage discrete time model proposed in Nathan's thesis [1].

- The model is not sensitive enough to L_0 , unlike what we obtained from the experiments. One may have a look at the parameters related with L_0 , or examine which parameters determine the disappear of oscillation the most.
- We are able to model the delayed oscillation in stress-time, but not seems possible for stress-strain without extreme parameters.

- Have a rigorous comparison on the critical compliance with the Toda's model, with experimental data involved as evidence. For details see Appendix B.
- Fit the model to more samples with experimental data, it is expected that only several parameters need to be changed. From this we know the certainty on many parameters can be confirmed.

More detailed experimental data extremely helps too. The following table summarises the experiments which can be considered at the moment.

Experiments	Effect & Sensitivity	Importance of experiment
Draw ratio λ	Qualitative effect; Quite sensitive.	Prior importance
Heat capacity c_p	Qualitative effect; Sensitive.	Great importance
Young's modulus E_1	The way to make stress decrease; Sensitive.	Important
Density ρ_0	Qualitatively effect; Sensitive.	Important
Neck front temperature	Beneficial to fit c_p, η .	Optional
Thermal map	The only way h_0, h_1 can be fitted.	Optional

Table 4.1: Suggested experiments for future study.

Nevertheless, the report implies that the generalised Toda's model is capable of doing quite accurate predictions to materials. There are ways to adjust the stress-strain curve freely, and rigorous fitting may require more experimental results for justify and require exploration at the universality on polymer films made by different materials.

Appendix A

Derivation: steady states of the new model

In case of needed, for example, to investigate predicted critical compliance of the new model in 3, one can refer to this appendix for the analytic steady states of the new model with density change. The analytic expression for steady state also has changes under our new density function $\rho(x)$. Now the temperature profile at steady state is:

$$\tau_s = \tau_s(0) \begin{cases} e^{(\xi_0 + \gamma_0)x}, & x < 0 \\ e^{(\lambda\xi_1 - \gamma_1)x}, & x > 0 \end{cases}$$

where $\xi_i = \rho_i c_p v_s / 2k_i$,

$$\gamma_0 = \frac{1}{2k_0} \sqrt{(\rho c_p v_s)^2 + 4h_0 k_0 \left(\frac{1}{a_0} + \frac{1}{b_0} \right)}, \quad \gamma_1 = \frac{1}{2k_1} \sqrt{(\rho c_p \lambda v_s)^2 + 4h_1 k_1 \left(\frac{1}{a_1} + \frac{1}{b_1} \right)},$$

and through integration of (1.2) over the infinitesimal interval $[-\epsilon, \epsilon]$ we can find our new $\tau_s(0)$:

$$\begin{aligned} \lim_{\epsilon \rightarrow 0} \int_{-\epsilon}^{\epsilon} \rho(x) c_p S_0 \tau_s(x) dx &= k_1 S_1 \frac{d\tau_s}{dx} \Big|_{0+} - k_0 S_0 \frac{d\tau_s}{dx} \Big|_{0-} + S_0 \eta \sigma_s (\lambda - 1) v_s \\ \implies 0 &= k_1 S_1 (\lambda \xi_1 - \gamma_1) \tau_s(0) - k_0 S_0 (\xi_0 + \gamma_0) \tau_s(0) + S_0 \eta \sigma_s (\lambda - 1) v_s \\ \implies [k_0 S_0 (\xi_0 + \gamma_0) - k_1 S_1 (\lambda \xi_1 - \gamma_1)] \tau_s(0) &= S_0 \nu (\lambda - 1) v_s \sigma_s \\ \implies \tau_s(0) &= \frac{S_0 \nu (\lambda - 1) v_s \sigma_s}{k_0 S_0 \gamma_0 - k_1 S_1 \gamma_1} \end{aligned}$$

Therefore the steady state $(\tau, |\dot{\chi}|, \sigma) = (\tau_s(x), v_s, \sigma_s)$ is the implicit solution to the following system:

$$\left\{ \begin{array}{l} \tau_s(x) = \frac{S_0 \nu (\lambda - 1) v_s \sigma_s}{k_0 S_0 \gamma_0 - k_1 S_1 \gamma_1} \exp \{ [(\xi_0 + \gamma_0) H(-x) + (\lambda \xi_1 - \gamma_1) H(x)] x \} \\ v_s = \frac{2v_0}{\lambda - 1} \exp \left\{ - \frac{\Delta F}{k_B (\tau_s(0) + T_a)} \right\} \sinh \left\{ \frac{\alpha \sigma_s}{k_B (\tau_s(0) + T_a)} \right\} \\ \sigma_s = E_0 \left(\lambda^2 \frac{\rho_1}{\rho_0} \frac{E_0}{E_1} - 1 \right)^{-1} \left\{ \frac{V}{v_s} - (\lambda - 1) \right\} \end{array} \right.$$

As previously, assuming $\sigma_s \ll E_0$ yields $v_s = V/(\lambda - 1)$.

Further approximating $\sinh(\cdot)$ by $\exp(\cdot)$ in the expression for v_s yields

$$\log(V/v_0) = \frac{\alpha \sigma_s - \Delta F}{k_B (\tau_s(0) + T_a)}$$

Therefore the new expression for the temperature at neck front at steady state is:

$$\tau_s(0) = \frac{\Delta F - k_B T_a \log(v_0/V)}{k_B \log(v_0/V) + \alpha(k_0 S_0 \gamma_0 + k_1 S_1 \gamma_1)/S_0 \nu V}$$

Appendix B

Comparison of predicted critical compliance

A large aspect of our research is to predict at which system compliance an oscillation in stress will occur. It's also mentioned as a future exploration. We have compared Toda's model and Nathan's model, along with a scatter simulation outcome by the latter model. It's ideal for us to do more experiments at different draw rates V , starting from samples of different initial lengths L_0 .

According to the definition of elastic compliance, $D(\chi; L_0) = \frac{\chi}{E_0} + \lambda^2 \frac{L_0 - \chi}{E_1}$, we know that initially $\chi = L_0$ so that $D(L_0; L_0) = \frac{L_0}{E_0}$, and in the end $\chi = 0$ so that $D(0; L_0) = \lambda^2 \frac{L_0}{E_1}$. By our investigation in Chapter 2, it's reasonable to assume that $\frac{E_1}{E_0} < \lambda^2$. So that as the neck propagates, equivalently χ decreases, D will increase monotonically.

To compare the two models by experimental data, we can set L_0 to be slightly less than $E_0 \cdot \min(D_{Toda}^*, D_{Nathan}^*)$ for each V we would like to investigate, where for example D_{Nathan}^* is the critical compliance obtained by bisection algorithm following Nathan's model.

In running Nathan's model, we used parameters fitted in Chapter 2.

k_0 (erg cm $^{-1}$ s $^{-1}$ K $^{-1}$)	k_1 (erg cm $^{-1}$ s $^{-1}$ K $^{-1}$)	E_0 (g cm $^{-1}$ s $^{-2}$)	E_1 (g cm $^{-1}$ s $^{-2}$)
1.50×10^4	3.70×10^4	2.25×10^{10}	6.1×10^{10}
h_i (erg cm $^{-2}$ s $^{-1}$ K $^{-1}$)	v_0 (cm s $^{-1}$)	α (cm 3)	ΔF (erg)
2.33×10^3	2.25×10^{72}	2.95×10^{-21}	8.55×10^{-12}
ρ (g cm $^{-1}$)	c_p (erg g $^{-1}$ K $^{-1}$)	λ	η
1.38	1.04×10^7	3.5	1

Table B.1: Parameters used in the generalised model for critical compliance prediction.

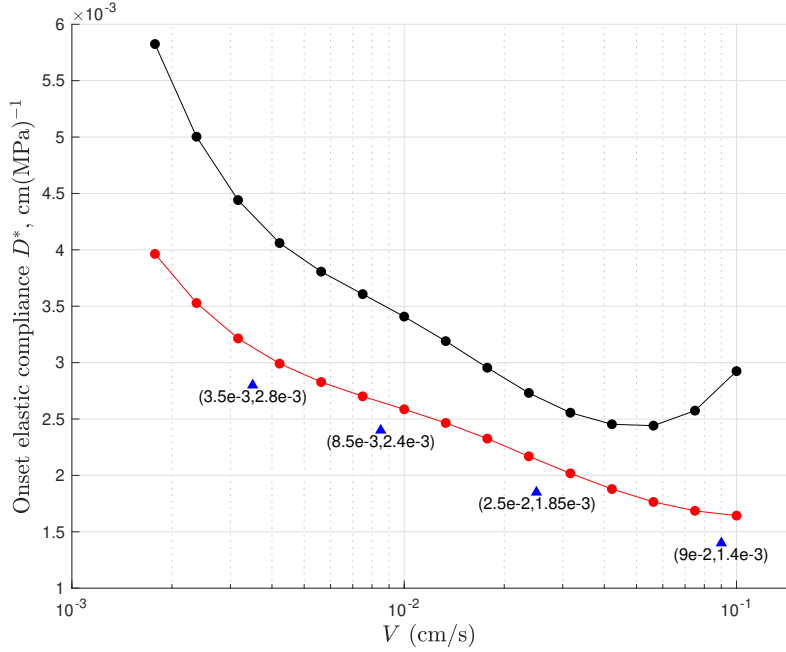


Figure B.1: The red scatters are our predictions on critical compliance following Nathan’s model, and the black scatters corresponds to Toda’s original model. The material is 0.5 wt % rGO. The blue triangles indicates the points we would like to test critical compliance.

We would like to conduct four experiments, starting from the blue triangles in Figure B.1. For example, for point $(3.5\text{e-}3, 2.8\text{e-}3)$ we draw a rGO sample of length $L_0 = E_0 \times 0.0028 = 6.3$ (cm) at constant draw rate 0.0035 cm/s. This method for comparison may not be valid, and thus needs justification or an alternative.

References

- [1] Nathan Coombs. Oscillatory neck propagation in polymer films. personal communication, 2021.
- [2] F. Ronkay and T. Czigány. Cavity formation and stress-oscillation during the tensile test of injection molded specimens made of PET. *Polymer Bulletin*, 57(6):989–998, August 2006.
- [3] A. Toda, C. Tomita, M. Hikosaka, Yu Hibino, H. Miyaji, C. Nonomura, T. Suzuki, and H. Ishihara. Thermo-mechanical coupling and self-excited oscillation in the neck propagation of pet films. *Polymer*, 43(3):947–951, 2001.
- [4] Akihiko Toda. Oscillation and instability of neck propagation in poly(ethylene terephthalate) films. *Polymer*, 34(11):2306–2314, 1993.
- [5] Akihiko Toda. Oscillatory neck propagation in polymer films: 2. *Polymer*, 35(17):3638–3642, 1994.
- [6] Lorenzo Torrisi, Mariapompea Cutroneo, Alfio Torrisi, and Letteria Silipigni. Measurements on five characterizing properties of graphene oxide and reduced graphene oxide foils. *physica status solidi (a)*, 219(6):2100628, 2022.
- [7] Chaoying Wan. All tensile data. personal communication, 2019.